4.1 VALIDATIONS OF THE NCEP MSM COUPLED WITH THE NOAH LSM OVER THE HAWAIIAN ISLANDS

Yi-Leng Chen[*] & Y.-X. Zhang
University of Hawaii, Honolulu, Hawaii

S.-Y. Hong
Yonsei University, Seoul, Korea

K. Kodama
National Weather Service Forecast Office, Honolulu, Hawaii

H.-M. H. Juang
National Centers for Environmental Prediction, Washington, D. C.

1. Introduction

The primary operational models for the NWSFO-HNL (National Weather Service Forecast Office – Honolulu) are the Aviation (AVN) and the Medium Range Forecast (MRF) runs of the Global Spectral Model (GSM). These model runs are generally able to provide forecast guidance on the synoptic-scale systems that affect the Hawaiian Islands; they are however unable to resolve the mesoscale weather features associated with the local complex terrain due to their coarse resolution. Recently, the NCEP (National Centers for Environmental Predictions) developed the high resolution Regional Spectral Model (RSM) (Juang and Kanamitsu 1994). In a collaborative effort among the University of Hawaii, NCEP and NWSFO-HNL, the hydrostatic version of the RSM with a 10-km resolution was implemented in early 1997 into the operational run stream for the state of Hawaii by NCEP. From preliminary analyses (Wang et al. 1998) and feedback from local forecasters, it is apparent that the RSM forecasts show improvements over the AVN and MRF runs in simulating heavy rainfall and high wind events. Nevertheless, there are still large discrepancies between the RSM simulations and observations because (1) the 10-km RSM grid is inadequate to resolve the local complex terrain, and (2) localized convections, resulting from the effects of topography, are not well represented by a hydrostatic model.

More recently, the nonhydrostatic version of the RSM (referred to as the Mesoscale Spectral Model; MSM) has been developed at NCEP (Juang 2000). In this model, both the hydrostatic perturbation in association with the external hydrostatic state and the nonhydrostatic perturbation related to the internally evolved hydrostatic state are introduced. The same model physics implemented in the RSM are used in the MSM without the hydrostatic assumption. It is shown in Juang (2000) that the MSM performs reasonably well in idealized and real case studies and is superior to the RSM with a coarse horizontal resolution of 50 km.

---
* Corresponding author address: Prof. Yi-Leng Chen, Department of Meteorology, University of Hawaii, Honolulu, HI 96822; email: yileng@hawaii.edu

Preliminary application of the MSM in Hawaii (Chen et al. 1999) shows encouraging results in simulating localized heavy rainfall and high winds.

In addition to the complex terrain, large variations in microclimate ranging from humid tropical on the windward lower slopes to hot desert over bare lava soil with different vegetation cover are typical for the Hawaiian Islands (Juvik et al. 1978). It has been recognized that land surface processes in association with heterogeneous vegetation and soil properties play a critical role in influencing the diurnal and vertical structure of the planetary boundary layer (PBL) and associated clouds and precipitation processes (Avissar and Pielke 1989; Chen and Avissar 1994a, b; Chen and Dudhia 2001a, b). However, in the current implementation of the RSM and MSM, only one vegetation type (broadleaf tree) is considered with a constant vegetation fraction of 70% over the entire Hawaiian Islands. It also uses only one soil type, sandy clay loam. This simple treatment of surface properties will inevitably lead to over-simplification of surface forcing which will probably result in erroneous model forecasts for surface variables. It is thus desirable to couple the RSM and MSM with an advanced land surface model (LSM) with improved lower boundary conditions to better resolve surface processes. In a collaborative effort among the University of Hawaii, the Yonsei University in Korea, and NWSFO-HNL, an earlier version of the NCEP operational NOAH (**N**CEP, **O**regon State University, **A**ir Force, and National Weather Service Office of **H**ydrology) LSM was implemented into the RSM and MSM in early 2002. The soil type, vegetation type and vegetation fraction at every grid point were compiled from the USGS Land Use Land Cover Datasets for Hawaii.

We have assessed the impacts of improved representation of the terrain and surface boundary conditions on simulating orographic and local effects under summer trade wind conditions, localized rainfall and orographically amplified high winds for a few cases (Chen et al. 1999; Zhang et al. 2000; Chen et al. 2002). Evaluation of the RSM and MSM coupled with the LSM is being made at NWS surface sites in Hawaii for a one-month period of May 20 through June 20 2002 using our archived model data from daily experimental forecasts. These results are briefly summarized in this

report. The structure of this report is as follows. Part 2 contains a brief description of the NCEP RSM, MSM, and the NOAH LSM. Model validations are presented in part 3. Conclusions and discussions are given in part 4.

2. Model description and design

2.1 RSM model and domain

A comprehensive description of the NCEP RSM is presented in Juang and Kanamitsu (1994). The current implementation of the RSM is either hydrostatic or nonhydrostatic with the latter generally referred to as the MSM. The primitive equations in sigma coordinates employed in the GSM are used in the RSM. While the GSM uses spherical harmonics functions, the RSM uses sine and cosine series as horizontal basis functions. The dependent variables in the regional domain are divided into a time-dependent base field and a perturbation part in terms of their spectral representation. The RSM then predicts deviations from the forecasts of the global model component. In other words, the RSM can resolve and predict those features not predicted by the GSM.

The model physics include short- and long-wave radiation with diurnal variation, radiation-cloud interaction, a surface layer with PBL physics, gravity-wave drag, simplified Arakawa-Schubert convective parameterization scheme, shallow convection, large-scale precipitation, and some hydrological processes (Kanamitsu 1980). To reduce noise from the lateral boundaries, a lateral boundary relaxation is performed on the total tendency computed in the RSM. A time filter (Asselin 1972) is applied to the perturbations in order to eliminate the computational mode resulting from a leapfrog time scheme in the integration. A semi-implicit adjustment is used for the perturbations in the regional domain to permit numerical stability with a large time step. An implicit horizontal diffusion was originally applied to the perturbations on sigma surfaces; however, such a numerical treatment was found to cause cold mountain-top air to spread downward and outward with model integration time in areas with steep terrain, which would eventually ruin model forecasts (Juang et al. 2003; submitted). This problem is corrected by implementing the horizontal diffusion for temperature and humidity on pressure surfaces instead. Horizontal diffusion for wind is still performed on sigma surfaces.

The entire RSM system designed for Hawaii consists of two components (Fig. 1): the GSM and the RSM. The RSM is nested into the GSM. The GSM component is a version of the operational NCEP Global Spectral Model. A 97×76-point grid domain is used for the RSM at a 10-km resolution. High-resolution (~ 1 km) Navy-NCAR terrain data for the Hawaiian Islands are used in the RSM. Since the RSM has the same model structure as the GSM, the initial conditions and lateral boundary conditions for the RSM are directly interpolated from the NCEP GSM run.

2.2 MSM model and domain

The MSM was developed based on fully compressible nonhydrostatic equations which were transformed from height coordinates to sigma coordinates under a hydrostatic base state. An externally determined hydrostatic coordinate was used in the earlier version (Juang 1992) but the internally evolved hydrostatic coordinate is employed in the current version (Juang 2000). This modification makes the MSM closer to the hydrostatic version in model structure and model dynamics. The major model physics employed in the RSM are used in the MSM without the hydrostatic assumption. A new precipitation physics package developed at NCEP (Hong et al. 1998b) has also been implemented into the MSM. This package incorporates a prognostic cloud scheme for the grid-resolvable precipitation and a parameterization convection scheme with a convective trigger function (Hong and Pan 1998a). Major numerical techniques in the MSM include spectral computation, time filter, semi-implicit adjustment for perturbation, and implicit horizontal diffusion for temperature and humidity (wind) on pressure (sigma) surfaces.

The entire MSM system designed for the Hawaiian Islands consists of three components: the GSM, the RSM, and the MSM. The first two components are the same as in the RSM system and have been described in section 2.1. The MSM component is nested into the RSM. The MSM is set up for three sub-regions of the state of Hawaii: the Oahu domain at a 1.5-km resolution, the Hawaii-Maui-Molokai domain at a 3-km resolution, and the Kauai domain at a 1.5-km resolution (Figs. 2a, 2b, 2c). The choice of resolution for the MSM domains is based on considerations of both cost-effectiveness and representation of major terrain features. In the 1.5-km Oahu domain (Fig. 2a), the model terrain adequately represents the two narrow mountain ranges (Koolau Range on the east and Waianae Range on the west). The peak height is 0.6 km for both mountain ranges in the model terrain which is about 0.3 km lower than the actual height. In the 3-km Hawaii-Maui-Molokai domain (Fig. 2b), both the Mauna Kea and Mauna Loa peaks over the island of Hawaii are evident with a height of 3.9 km, which is only about 0.2-0.4 km lower than the actual height. The peak height of the Haleakala mountain on the island of Maui is roughly 2.7 km in the MSM domain, about 0.3 km lower than the actual height. The terrain features of two small islands, Lanai and Kahoolawe, are also evident in the 3-km model domain. Lastly, the 1.5-km Kauai domain (Fig. 2c) reasonably resolves the mountain shape with a peak height of 1.3 km, comparable to the actual height of 1.5 km. This model domain also resolves the Waimea Canyon located southwest of the mountain ridge and another small mountain over the island of Niihua, situated southwest of the island of Kauai.
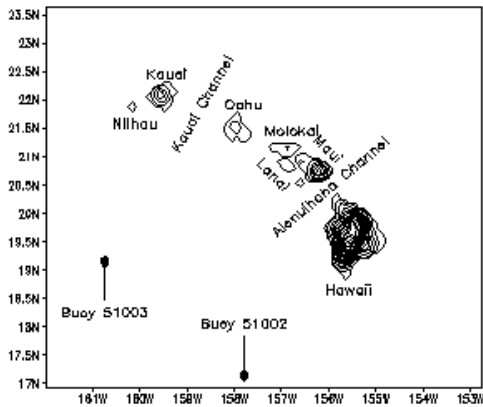
Fig. 1 The domain of the Regional Spectral Model (RSM) for the state of Hawaii at a 10-km resolution. The terrain contour interval is 200 m.
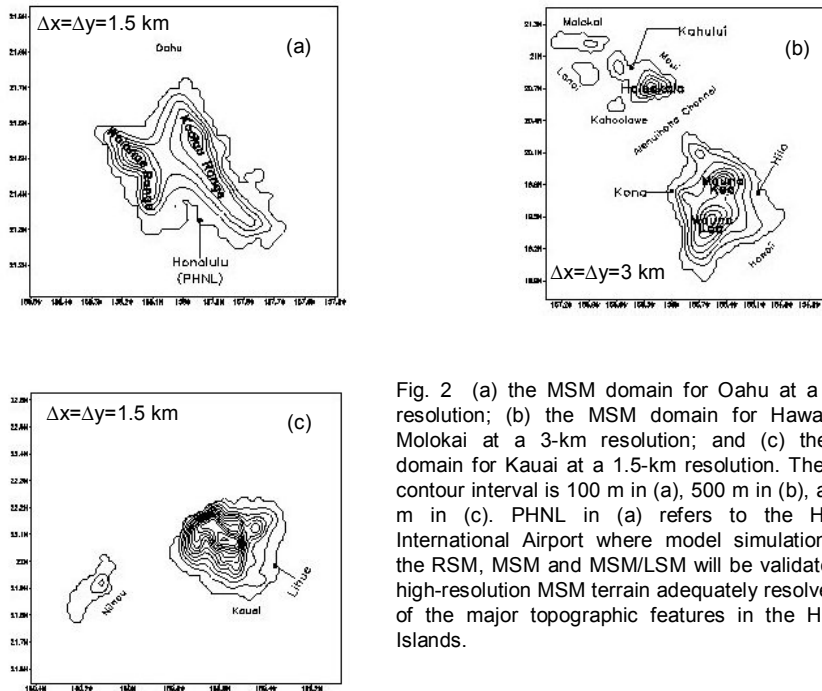

Fig. 2 (a) the MSM domain for Oahu at a 1.5-km resolution; (b) the MSM domain for Hawaii-Maui-Molokai at a 3-km resolution; and (c) the MSM domain for Kauai at a 1.5-km resolution. The terrain contour interval is 100 m in (a), 500 m in (b), and 100 m in (c). PHNL in (a) refers to the Honolulu International Airport where model simulations from the RSM, MSM and MSM/LSM will be validated. The high-resolution MSM terrain adequately resolves most of the major topographic features in the Hawaiian Islands.

2.3 NOAH LSM

The LSM coupled with the current version of the RSM and MSM uses an earlier version of the NOAH LSM implemented in the NCEP operational meso Eta model. The NOAH LSM web site is located at http://www.emc.ncep.noaa.gov/mmb/gcp/noahlsm/README-2.2.htm.

The current implementation of the NOAH LSM has a two-layer soil model (Mahrt and Pan 1984; Pan and Mahrt 1987) with 0.1-m and 1.9-m thick layers, and it also has a distribution of soil types. Soil parameters and vegetation parameters are specified at each grid point. 16 soil categories and 13 vegetation categories are used in the model. Vegetation fraction ranges from 0 to 100%. Surface albedo, roughness length, and deep soil temperature are computed based on the vegetation type at each grid point. SST field is directly interpolated from daily analyses which can be downloaded from ftp://polar.wwb.noaa.gov. The NOAH LSM simulates soil moisture (both liquid and frozen), soil temperature, skin temperature, snowpack depth, snowpack water equivalent (and hence snowpack density), canopy water content, and the energy flux and water flux terms of the surface energy balance and surface water balance. The surface data for the NOAH LSM were compiled from the 1:100,000-scale Land Use Land Cover Datasets for Hawaii (DOI USGS 1986).

3. Results

3.1 Under summer trade wind conditions

We have been running the experimental MSM for the Oahu domain at a 1.5-km resolution daily since late 2000 and the MSM/LSM run since early 2002. Validations of the MSM/LSM simulations are carried out at the Honolulu International Airport (PHNL) within the Oahu domain for the period of May 20 through June 20 2002. The location of PHNL is shown in Fig. 2a. We looked at 2-m temperature, 2-m dew point temperature, 10-m wind speed and 10-m wind direction. The period of May 20 through June 20 2002 can be characterized by first 10-day's weak synoptic winds due to the proximity of the subtropical ridge to the Hawaiian Islands followed by normal trade wind weather brought by the subtropical ridge then located to the north of the islands (not shown).

Fig 3 shows the observed and 12-h RSM, MSM and MSM/LSM predicted (a) 2-m temperature and (b) 2-m dew point temperature valid at 0200 HST for PHNL during the period of May 20 through June 20 2002. "OBS" refers to observations. "R12", "M12" and "ML12" refer to the 12-h forecast by the RSM, MSM and MSM/LSM, respectively. Notice that the RSM generally forecasts higher surface temperature at nighttime than observations (Fig. 3a). Our ensuing investigation reveals that in the RSM domain with a 10-km resolution, PHNL is treated as an ocean point instead of as a land point. Thus, nighttime cooling effect is not taken into account at PHNL in the RSM domain. The MSM/LSM and MSM simulated surface temperature are close to each other and are consistent with observations especially under normal trade wind conditions during May 31 to June 20, but large discrepancies exist between model simulations and observations under weak wind conditions during May 20 thought May 30 (Fig. 3a). In terms of 2-m dew point temperature at 0200 HST (Fig. 3b), the RSM simulations are persistently higher than observations probably due to its treatment of PHNL as an ocean point; while the MSM/LSM and MSM simulated 2-m dew point temperature is generally consistent with observations.

Fig. 4 is the same as Fig. 3 but for the 24-h RSM, MSM and MSM/LSM predictions valid at 1400 HST. The RSM, MSM and MSM/LSM simulations diverge considerably. The RSM and MSM persistently forecast lower 2-m temperature than observations on almost all days with the difference as large as 4 ºC (2 ºC) for RSM and 3 ºC (1 ºC) for MSM during normal trade wind (weak wind) days (Fig. 4a). As mentioned before, PHNL is treated as an ocean point in the RSM domain and thus daytime heating effect is not accounted for in the RSM simulations for PHNL. As for the uncoupled MSM, it appears to contain notable cold bias during daytime. In comparison, the 2-m temperature forecast by the MSM/LSM matches observations quite well during normal trade wind period and is reasonably well during weak wind period (Fig. 4a). This improved performance of the MSM/LSM over the MSM at 1400 HST is likely attributable to better representation of land surface

forcing by the LSM. Related with ocean point treatment and cold bias in the RSM and MSM simulations, both models also predict higher (3-4 ºC higher) 2-m dew point temperature than the observed at 1400 HST for PHNL (Fig. 4b). As mentioned before, there is only one vegetation type (broadleaf tree) with a constant vegetation fraction of 70% over the entire Hawaiian Islands in the MSM; however, in reality, PHNL is located in an urban area with less than 10% vegetation cover. This implies that surface moisture at PHNL is overestimated by the MSM during daytime as well, which may also have contributed to higher dew point temperature in the MSM simulations. Notice that the MSM/LSM provides a close fit to observations (Fig. 4b).

Fig. 5 shows the observed and 12-h RSM, MSM and MSM/LSM predicted (a) 10-m wind direction and (b) 10-m wind speed valid at 0200 HST for PHNL during the period of May 20 through June 20 2002. It can be seen that all three models produce identical forecasts for 10-m wind direction during normal trade wind days which are generally conform to observations (Fig. 5a), with appreciable discrepancies between model simulations and observations occurring during weak wind period when land surface forcing becomes more important. In terms of 10-m wind speed (Fig. 5b), the RSM (MSM) simulations are about 5 m s^{-1} (4 m s^{-1}) higher than observations during normal trade wind days. In other words, the RSM and MSM significantly overestimate the surface wind speed. Our further investigation reveals that surface roughness in the RSM and MSM, which is ultimately interpolated from the AVN data, is unrealistically small (0.005 – 0.01 m) over the entire Hawaiian Islands. This small surface roughness is believed to give rise to higher than observed surface wind speed in the RSM and MSM simulations. In comparison, the MSM/LSM simulated 10-m wind speed at 0200 HST is generally close to observations mainly due to its realistic specification of surface roughness by the LSM.

Fig. 6 is the same as Fig. 5 but for the 24-h RSM, MSM and MSM/LSM simulations valid at 1400 HST. Notice that the MSM/LSM captures the observed onshore wind component (wind direction ≥ 90º) during weak wind days while the RSM and MSM do not (Fig. 6a). The RSM and MSM also over-estimate the observed 10-m wind speed by about 3 m s^{-1} during normal trade wind days (Fig. 6b). In comparison, the MSM/LSM provides a close fit to the observed 10-m wind speed especially during normal trade wind days.

We have also plotted composite horizontal maps of surface wind for weak trade wind days in the nested Oahu domain to further evaluate the performance of the MSM/LSM and MSM in capturing the afternoon sea breezes under weak synoptic wind conditions when land surface forcing is more important. We define weak trade wind days as when (1) upstream wind speed is smaller than 5 m s^{-1}, and (2) upstream winds are blowing from east most time of the day. Basing on these two criteria, we have selected three weak trade wind days, 5/24, 5/25 and 5/26, during the period of May 20 through June 20 2002. Fig. 7 shows the analyses valid at 1400 HST constructed from the

MSM/LSM and MSM simulations. It can be seen that the MSM/LSM resolves onshore wind component (sea breezes) along the coastlines surrounding the island; while the MSM provides weak onshore flow only along the eastern and western coastline. Considering that there are considerable cold biases in the MSM simulations over land at 1400 HST (Fig. 4a), it is not surprising to note that the MSM dose not resolve afternoon sea breezes quite well.
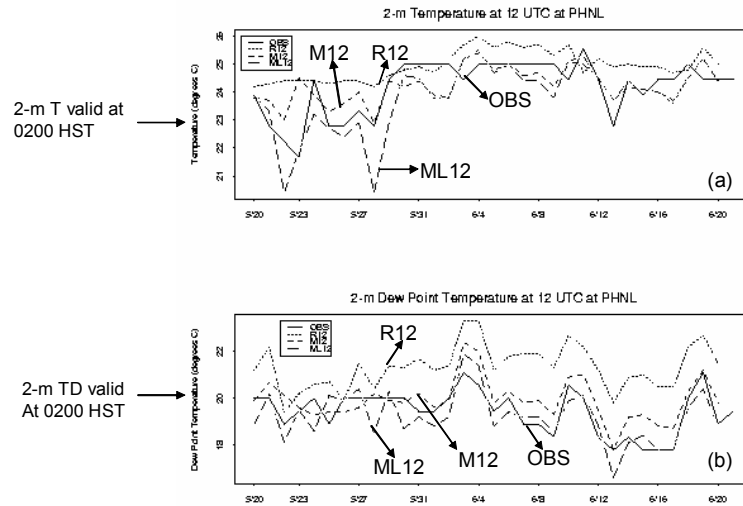
2-m T valid at 0200 HST →

2-m TD valid At 0200 HST →

Fig. 3 Observed and 12-h model prediction valid at 0200 HST for Honolulu Airport (PHNL) during the period of May 20 through June 20 2002 (a) 2-m temperature and (b) 2-m dew point temperature. Unit is °C. "OBS" refers to observations; "R12", "M12", and "ML12" refer to the 12-h forecast by the RSM, MSM, and MSM/LSM, respectively. The RSM, MSM and MSM/LSM runs were initialized at 1400 HST each day. The coupled MSM/LSM forecasts were the closest to observations both in (a) and (b). The 2-m dew point temperature predicted by the RSM was persistently 2-3 °C higher than the observed in (b).
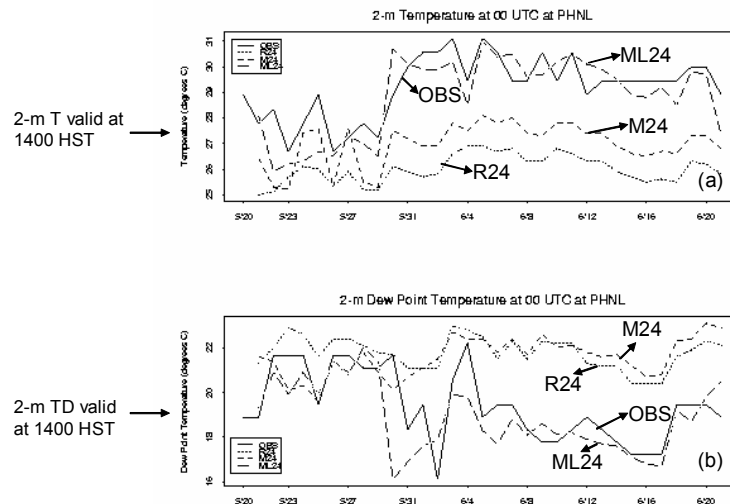
2-m T valid at 1400 HST →

2-m TD valid at 1400 HST →

Fig. 4 Observed and 24-h model prediction valid at 1400 HST for Honolulu Airport (PHNL) during the period of May 20 through June 20 2002 (a) 2-m temperature and (b) 2-m dew point temperature. Unit is °C. "OBS" refers to observations; "R24", "M24", and "ML24" refer to the 24-h forecast by the RSM, MSM, and MSM/LSM, respectively. The RSM, MSM and MSM/LSM runs were initialized at 1400 HST each day. Notice the under-estimation (over-estimation) of 2-m temperature (2-m dew point temperature) by the RSM and the uncoupled MSM. The coupled MSM/LSM forecasts were consistent with observations.

10-m Wind Direction at 12 UTC at PHNL

10-m WD valid at 0200 HST →

M12   →R12

ML12

→OBS

(a)

10-m Wind Speed at 12 UTC at PHNL

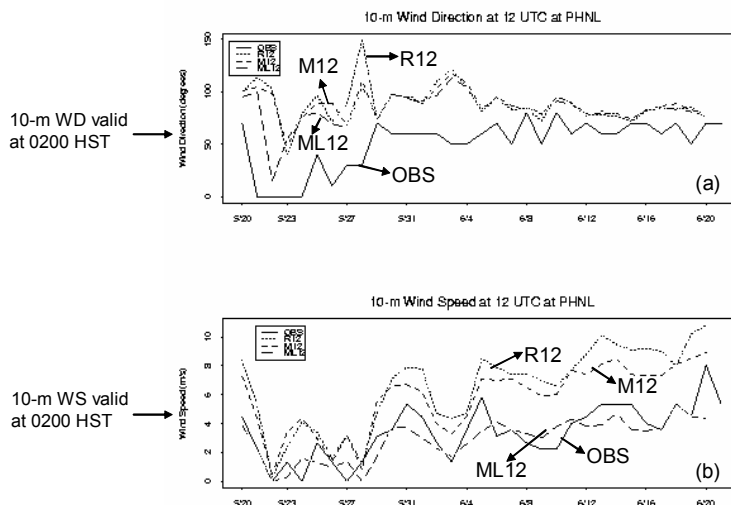10-m WS valid at 0200 HST →

→R12

→M12

ML12   →OBS

(b)

Fig. 5 Observed and 12-h model prediction valid at 0200 HST for Honolulu Airport (PHNL) during the period of May 20 through June 20 2002 (a) 10-m wind direction and (b) 10-m wind speed. Unit is degrees for wind direction and m s⁻¹ for wind speed. "OBS" refers to observations; "R12", "M12", and "ML12" refer to the 12-h forecast by the RSM, MSM, and MSM/LSM, respectively. The RSM, MSM and MSM/LSM runs were initialized at 1400 HST each day. All the model performance was comparable in simulating the 10-m wind direction; however, the 10-m wind speed was best reproduced by the coupled MSM/LSM.
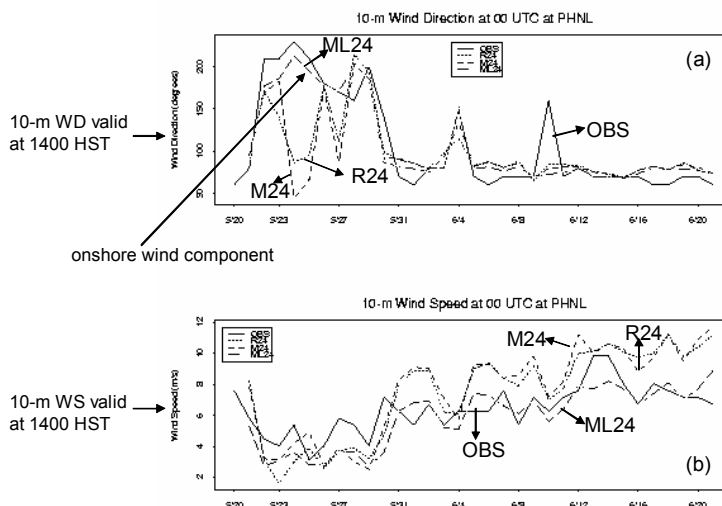
10-m Wind Direction at 00 UTC at PHNL

10-m WD valid at 1400 HST →

ML24

(a)

→OBS

M24   R24

onshore wind component

10-m Wind Speed at 00 UTC at PHNL

10-m WS valid at 1400 HST →

M24←   R24

ML24

OBS

(b)

Fig. 6 Observed and 24-h model prediction valid at 1400 HST for Honolulu Airport (PHNL) during the period of May 20 through June 20 2002 (a) 10-m wind direction and (b) 10-m wind speed. Unit is degrees for wind direction and m s⁻¹ for wind speed. "OBS" refers to observations; "R24", "M24", and "ML24" refer to the 24-h forecast by the RSM, MSM, and MSM/LSM, respectively. The RSM, MSM and MSM/LSM runs were initialized at 1400 HST each day. The trade winds were weaker than normal during the early part of the period with a pronounced onshore wind component at 1400 HST best simulated by the coupled MSM/LSM.

3.2 Two heavy rainfall cases

3.2.1 Nov. 1-2 2000 flood on the island of Hawaii

During 1-2 November 2000 a line of thunderstorms with a northeast-southwest orientation brought heavy rains to the island of Hawaii. Between 1400 HST 1 November and 1400 HST 2 November, the southeast part of the island and Hilo area reported rainfall of more than 700 mm with amounts in excess of 900 mm at Kapala Range on the east rift of Mauna Loa (Fig. 8). The downpour overflowed stream and gullies, flooded roadways throughout the downtown Hilo area and cut off several neighborhoods along the east side of the island. The heavy rains also caused several landslides and disrupted telephone services. Most electrical customs on the island endured hours of power failures. The total damage was estimated at $70 million.
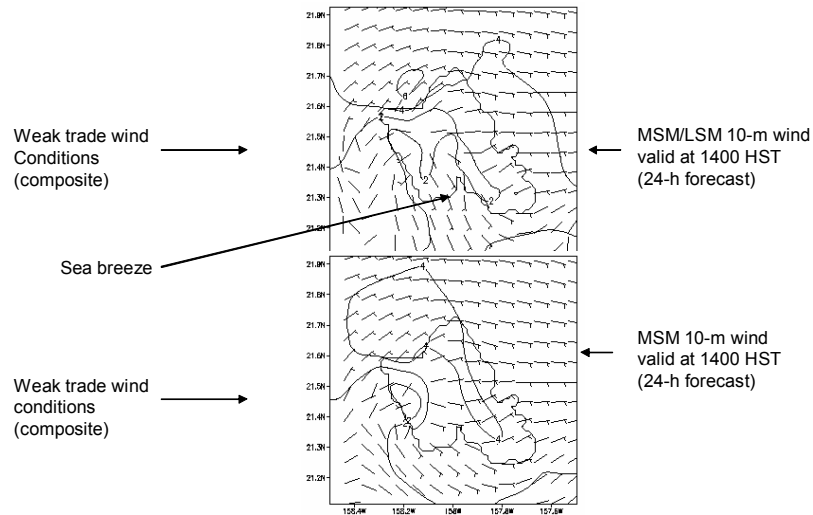
Fig. 7 Composite horizontal maps of 10-m wind (m s^{-1}) for the Oahu domain simulated by (a) the coupled MSM/LSM and (b) the uncoupled MSM valid at 1400 HST for the weak trade wind days (defined as when wind speed < 5 m s^{-1}). Isotach is drawn for every 2 m s^{-1}. Half barb and full barb denote 5 m s^{-1} and 10 m s^{-1}, respectively. The models were initialized at 1400 HST the previous day. Notice that the MSM/LSM captured the sea breezes much better than the MSM.
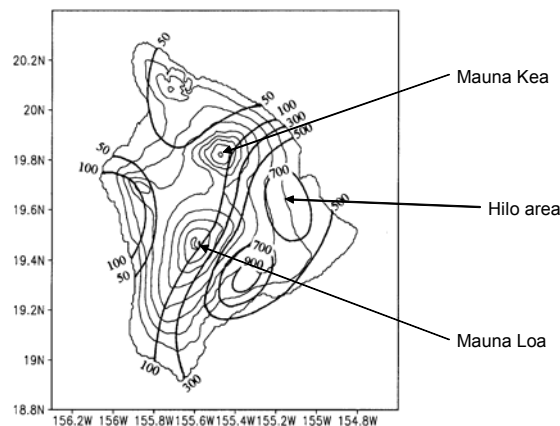

Fig. 8 Observed 24-h accumulated rainfall (mm) from 1400 HST November 1 to 1400 HST November 2 2000. Contours are drawn for 50, 100, 300, 500, 700, and 900 mm. The southeast part of the island and the Hilo area reported rainfall of more than 700 mm with amounts in excess of 900 mm recorded on the southeast rift of the Mauna Loa.

The 250-hPa height and wind analyses for 1400 HST 1 November 2000 (Fig. 9a) show a cut-off low to the southwest of the Hawaiian Islands. A subtropical westerly jetstream with maximum wind speed in excess of 40 m s^{-1} was evident to the east of the cut-off low. This cut-off low drifted slowly away from the Hawaiian Islands within the next 24-h period (not shown). The associated surface cyclogenesis is consistent with a class of subtropical cyclones known as Kona lows (Simpson 1952; Ramage 1962), as was evidenced in the surface analyses from 1400 HST 1 November 2000 which show the establishment of an inverted trough south of the Hawaiian Islands (Fig. 9b). Also evident in Fig. 9b was a mid-latitude cold front located some 800 km to the northwest of the Hawaiian Islands. This cold front was trailing behind the subtropical high situated to the northeast of the Hawaiian Islands. Under this synoptic configuration, the Hawaiian Islands were located on the anticyclonic side of the entrance region of the westerly jetstream in the upper troposphere and
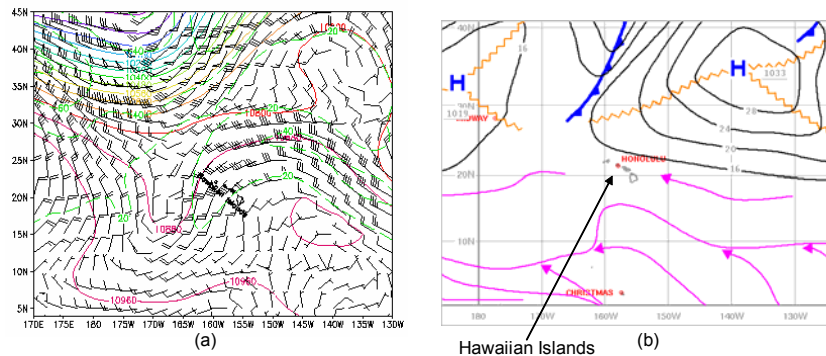
Fig. 9 (a) 250-hPa geopotential height (gpm, solid lines) and winds (m s^{-1}, barbs and dashed lines) analyses based on the NCEP/NCAR Reanalyses Data for 1400 HST November 1 2000; (b) surface analyses for 1400 HST November 1 2000 (adapted from the subjective analyses by forecasters at the National Weather Service Forecast Office, Honolulu). Isotaches in (a) are plotted for every 20 m s^{-1}. Isobars in (b) are plotted for every 4 hPa. This wintertime Kona storm brought heavy rains to the island of Hawaii (Big Island). Notice that the surface southeasterly was subject to orographic lifting on the southeastern portion of the Big Island.

were under the influence of southerly flows at the low levels. The resulting divergence aloft and the lower level convergence between the southeasterly winds blowing from the subtropical high and the southwesterly winds blowing from the frontal system combined together with local orographic lifting placed the southeast part and Hilo area of the island of Hawaii in the most favorable situation for deep convection and thunderstorm activity.

This Kona storm was also fueled by the remnants of Tropical Storm Paul (not shown), which developed in the inter-tropical convergence zone (ITCZ) off the west coast of Mexico on 22 October 2000. Surface analyses and satellite images indicated that Paul became a tropical storm on the 26th and dissipated by the 29th after traveling about halfway to the Hawaiian Islands. Its remnants continued westward movement and, as they approached the island of Hawaii on 1 November, they were amplified by the above-mentioned upper-level low system located to the southwest of the islands.

The 10-km RSM and the 3-km MSM/LSM simulations for this case were initialized at 0200 HST 1 November 2000, ~ 17 hours prior to the heaviest rainfall. Fig. 10a shows the 24-h accumulated rainfall ending at 1400 HST 2 November predicted by the RSM. Note that the RSM forecast heavy rainfall was mainly located over the two mountain tops (Mauna Kea and Mauna Loa) on the island of Hawaii and that the simulated maximum rainfall amount of 230 mm was only about one fourth of the recorded maximum rainfall amount of 900 mm. The reason that the RSM predicted the heaviest rainfall over the two mountain tops instead of on the southeastern part of the island as in observations is that the 10-km RSM only partially resolves the low level convergence and orographic lifting. This is demonstrated in Fig. 10b

which shows the RSM simulated 10-m wind valid at 1400 HST November 2 2000. Convergence in wind speed is evident over the Hilo area in Fig. 10b but the southeastern part of the island corresponds to neither convergence nor orographic lifting as air flow is largely deflected along the coastline before reaching the slopes. This abrupt deflection of air flow along the coastline may be due to the steepened terrain in the 10-km grid. Another factor in this large discrepancy is that localized convection in the Hawaiian Islands results primarily from the effects of topography and should be better resolved by a nonhydrostatic version of the RSM. In association with the low-level speed convergence in the Hilo area and local orographic lifting, the 10-km RSM predicted appreciable rainfall there but the rainfall amount was still well below the observed amount (80 mm verses 700 mm). In comparison, the 3-km MSM/LSM predicted heavy rainfall over the southeast part and the Hilo area with a maximum rainfall amount of 550 mm for both areas (Fig. 11a), in general agreement with the observed rainfall distribution. In the corresponding 10-m wind field constructed from the MSM/LSM simulations valid at 1400 HST November 2 (Fig. 11b), convergence in wind speed and orographic lifting are apparent over the southeastern part and Hilo area of the island of Hawaii. The 3-km MSM/LSM also forecasted considerable rainfall over the northeastern and southern parts of the island, consistent with the observed rainfall pattern (cf. Fig. 11a and Fig. 8). The significant improvements in air flow and rainfall simulations by the MSM/LSM over the RSM demonstrates the necessity of using high-resolution, nonhydrostatic mesoscale models to resolve the island effect in heavy rainfall events.
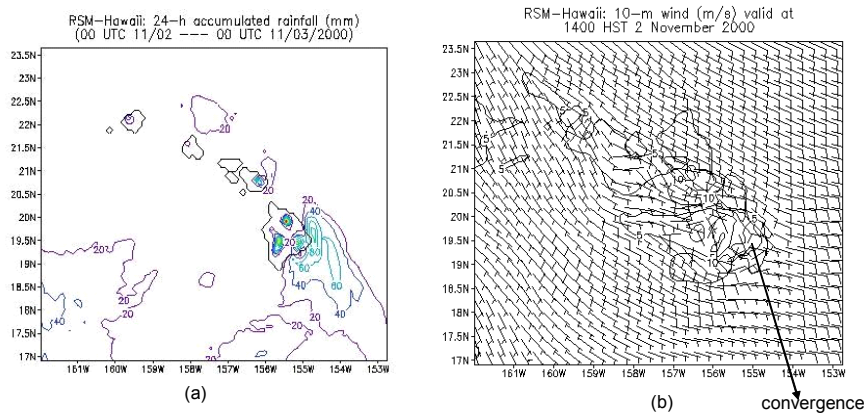
RSM−Hawaii: 24−h accumulated rainfall (mm)
(00 UTC 11/02 −−− 00 UTC 11/03/2000)

RSM−Hawaii: 10−m wind (m/s) valid at
1400 HST 2 November 2000

(a)

(b) convergence

Fig. 10 (a) RSM forecast 24-h accumulated rainfall (mm) from 1400 HST November 1 to 1400 HST November 2 2000, (b) RSM forecast 10-m wind (m s^{-1}) valid at 1400 HST November 2 2000. Contour interval is 20 mm in (a) and 5 m s^{-1} in (b). The RSM was initialized at 0200 HST November 1 2000. The RSM predicted heavy rains mainly over the two summits (Mauna Kea and Mauna Loa) and the Hilo area with a rainfall amount of 80 – 120 mm. These rainfall areas correspond quite closely to convergence areas in wind speed in the 10-m wind field in (b).
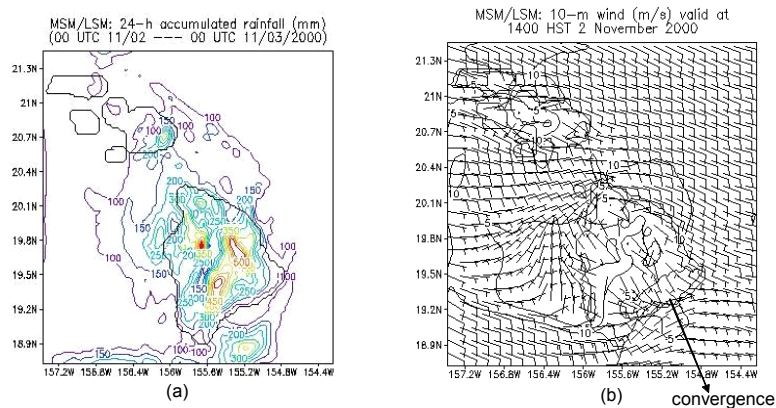

MSM/LSM: 24−h accumulated rainfall (mm)
(00 UTC 11/02 −−− 00 UTC 11/03/2000)

MSM/LSM: 10−m wind (m/s) valid at
1400 HST 2 November 2000

(a)

(b) convergence

Fig. 11 (a) MSM/LSM forecast 24-h accumulated rainfall (mm) from 1400 HST November 1 to 1400 HST November 2 2000; (b) MSM/LSM forecast 10-m wind (m s^{-1}) valid at 1400 HST November 2 2000. Contour interval is 50 mm in (a) and 5 m s^{-1} in (b). The MSM/LSM was initialized at 0200 HST November 1 2000. The MSM/LSM predicted heavy rains over the southeast part and Hilo area on Big Island, consistent with the observed rainfall distribution. Convergence in wind speed and orographic lifting are apparent over the southeast part and Hilo area.

3.2.2 November 2-3 1995 heavy rainfall event on the island of Kauai

During the late morning hours of 3 November 1995, a line of thunderstorms with a northeast-southwest orientation in association with a Kona low system brought heavy rainfall to most of the island of Kauai. Between 1400 HST 2 November and 1400 HST 3 November, the north and east sides of the island recorded rainfall of 200 – 250 mm, while the south and west sides of the island received 50 – 100 mm of rain (Fig. 12). The heavy rains caused flooding in several areas from the northern to the eastern portions of the island, resulting in road closures and evacuations. Low ceilings, poor visibility, and erratic winds during this event resulted in the cancellation of 17 flights between the islands of Kauai and Oahu. Monetary losses from the flooding were estimated at $685,000.
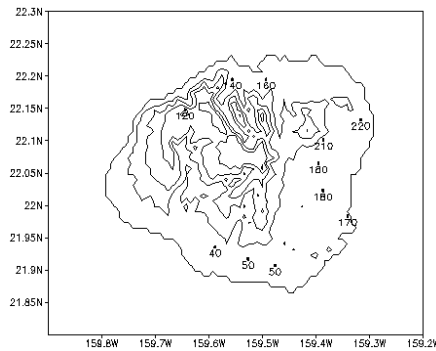
Fig. 12 Observed 24-h accumulated rainfall (mm) from 1400 HST November 2 to 1400 HST November 3 1995 on the island of Kauai. Only station values are plotted. Heavy rains were observed on the lee side of the island with the heaviest rainfall (~ 220 mm) recorded on the northeastern part of the island. The windward side also received considerate amount of rainfall.
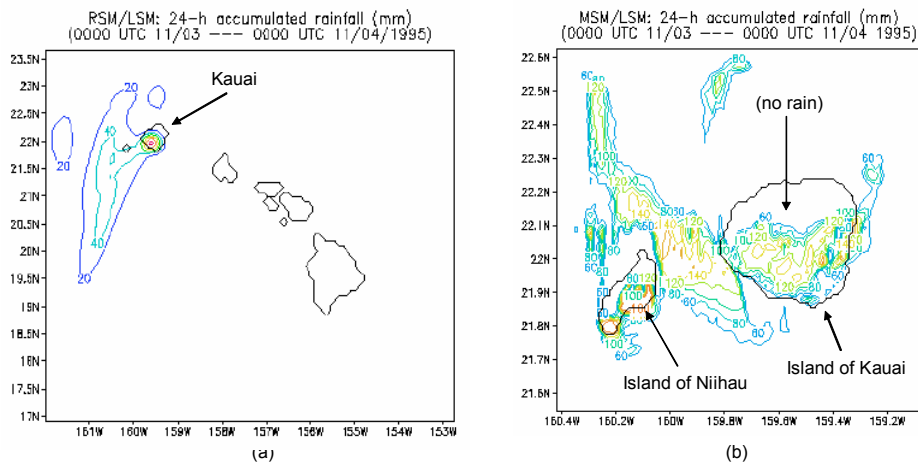

Fig. 13 24-h accumulated rainfall (mm) from 1400 HST November 2 to 1400 HST November 3 1995: (a) 10-km RSM/LSM forecast, and (b) 1.5-km MSM/LSM forecast. Contour interval is 20 mm in both (a) and (b). The models were initialized at 1400 HST November 2 1995. The heaviest rainfall amount in (a) was only one-third of the observed rainfall amount. The MSM/LSM forecast heaviest rainfall of 200 mm on the eastern part of the island, in general consistence with observations. Notice that both the RSM/LSM and the MSM/LSM did not generate the observed large amount of rainfall on the lee side of the island.

The synoptic and mesoscale environment associated with the severe weather brought by this Kona low and the formation of a bow echo detected by the then newly-installed WSR-88D radar on the south shore of the island have been discussed extensively in Businger et al. (1998). Wang et al. (1998) contrasted the AVN forecast and the nested RSM forecast for this heavy rainfall event and they concluded that while the RSM output provided much better 24-h forecast guidance than the AVN, the rainfall amount predicted by the RSM was only one-third of that observed and the area of heavier rainfall was forecast over the southern half of the island instead of over the northeastern section of the island as shown in observations. They suggested that the local convection, resulting from large-scale flow interaction with the island terrain that involves local-scale and nonhydrostatic processes, were not well handled by the RSM at a resolution of 10 km.
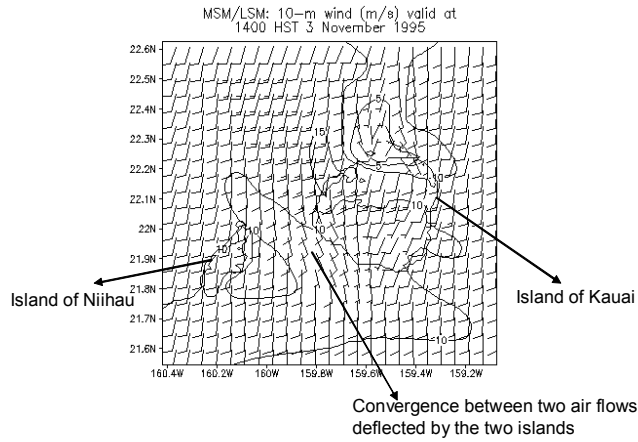
MSM/LSM: 10-m wind (m/s) valid at
1400 HST 3 November 1995

Island of Niihau

Island of Kauai

Convergence between two air flows
deflected by the two islands

Fig. 14 10-m wind (m s^{-1}) predicted by the MSM/LSM valid at 1400 HST November 3 1995. Contour interval is 5 m s^{-1}. The MSM/LSM was initialized at 1400 HST November 2 1995. Notice the convergence in wind direction between air flows deflected by the island of Niihau in the west and the island of Kauai in the east. There is also apparent convergence in wind direction over the eastern part of the island of Kauai. Air flow over the southern part of the island of Kauai subjects to orographic lifting.
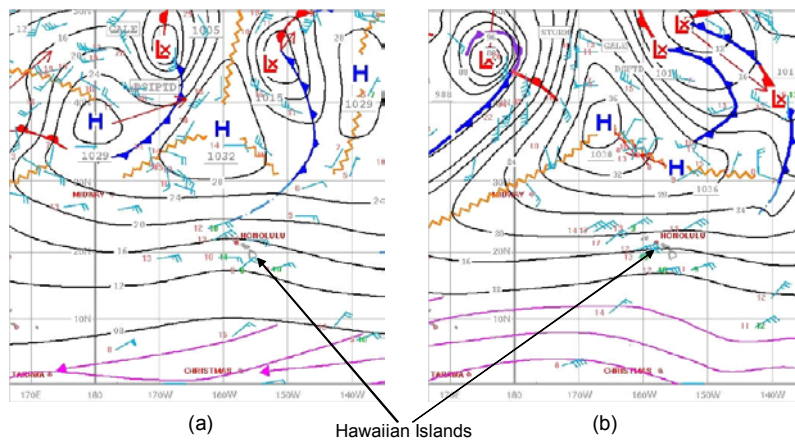

(a)

Hawaiian Islands

(b)

Fig. 15 Surface analyses for 1400 HST on (a) February 13 and (b) February 14 2001 (adapted from the subjective analyses by forecasters at the National Weather Service Forecast Office, Honolulu). Isobars are plotted for every 4 hPa. Notice that a strong subtropical high moved to the north of the Hawaiian Islands following the passage of a cold front (a). This high, reaching its maximum strength of 1038 hPa by 1400 HST February 14 (b), brought in strong trade winds across the state of Hawaii.

Our RSM/LSM and MSM/LSM simulations for this case were initialized at 1400 HST 2 November 1995, ~ 18 h prior to the heaviest rainfall. Instead of doing two nests as in Wang et al. (1998), we applied direct nesting from the GSM to the 10-km RSM/LSM. We noted that direct nesting from the GSM to the 10-km RSM/LSM produced identical simulations to those by doing two nests as illustrated in Fig. 13a which shows almost the same rainfall distribution as in Wang et al. (1998). In comparison, the 1.5-km MSM/LSM provides a much closer rainfall pattern (Fig. 13b) to observations than the RSM/LSM. The MSM/LSM forecasted heaviest rainfall of amount of 150 – 200 mm on the eastern part of the island and heavier rainfall of amount of 100 – 150 mm on the southern part of the island, in consistence with observations. This also agrees with the flow pattern in the MSM/LSM simulations which show that the eastern part of the island of Kauai corresponds to flow convergence between the air flow deflected by the island and the air flow passing through the Kauai

Channel while southerly air flow over the southern part of the island subjects to apparent orographic lifting (Fig. 14). However, one shortcoming in the MSM/LSM simulations for this case is that, contrary to observations, the model predicted no rainfall on the leeside of the island (Fig. 13b), the reason of which is still under investigation. Significant rainfall (~ 60 mm) is also evident on the windward side of the small island of Niihau and over the open oceans between the islands of Niihau and Kauai (Fig. 13b). The rainfall on the windward side of the island of Niihau appears to be the result of orographic lifting to the southerly flow; while the rainfall over the open oceans between the two islands is likely related to the convergence of the deflected air flows by these two neighboring islands (see Fig. 14). The WSR-88D radar image from 1400 HST 3 November 1995 (Fig. 7 in Businger et al. 1998) also indicted convective activities in these areas.

3.3 A high wind event

During the period of February 13 – 14 2001, a strong subtropical high moved to the north of the Hawaiian Islands following the passage of a cold front (Fig. 15a). This high, reaching its maximum strength of 1038 hPa by 1400 HST February 14 2001 after merging with a trailing high cell (Fig. 15b), produced strong winds that knocked down trees and disrupted power in many island communities. Newspapers reported most of the power failures and damages on the lee sides of mountain ranges with tops below the trade wind inversion (~ 1500 m) as well as within saddles between mountain ranges. Gale warnings were issued at 0400 HST 14 February for all oceanic channels by the National Weather Service. In addition to high winds, showery activities were reported everywhere in Hawaii except on the lee sides of high mountains of Maui and the island of Hawaii. For brevity, our discussion for this high wind case focuses on the Oahu domain.

The RSM/LSM and MSM/LSM runs for this case were initialized at 1400 HST 13 February 2001. Fig. 16a shows the horizontal map of 10-m wind simulated by the RSM/LSM valid at 1800 HST 14 February. The reason we chose 1800 HST is that the RSM/LSM-predicted upstream surface wind speed peaked around this time as illustrated in the time-latitude cross section along 154 °W presented in Fig. 16b. General features in Fig. 16a include (1) weak winds on the windward side of mountain ranges due to island blocking; (2) wake areas on the lee side of major islands; and (3) strong winds at the southern and northern corners of major islands as well as within the Alenuihaha Channel. Wind pattern on Kauai and Oahu is quite uniform due to the coarse representation of the island terrain by the 10-km model grid.

Fig. 17a shows the horizontal distribution of 10-m wind simulated by the 1.5-km MSM/LSM for the Oahu domain. Relatively weak winds (< 10 m s^{-1}) are located on the windward side of the Koolau Range and Waianae Range, due to mountain blocking. Orographically-enhanced winds (~ 12 m s^{-1}) are identified along the lee slopes of the two mountain ranges, in agreement with newspaper reports. The open oceans immediately off the northern and southern coast of the island experience strong winds of 16 m s^{-1}. We also constructed a longitude – height cross section along OA-OB (see Fig. 17a for its location) showing the MSM/LSM forecast horizontal wind field and potential temperature. The result is presented in Fig. 17b. The model terrain in this cross section is characterized by two north-south running mountain ranges, Koolau Range in the east and Waianae Range in the west, with similar peak height of 0.6 km. This height is about 0.3 km lower than the actual height. Fig. 17b reveals strong downslope winds along the lee slopes of both mountain ranges, in consistent with damage report. The strongest winds with wind speed in excess of 22 m s^{-1} are located roughly 200 m above the surface. Potential temperature distribution in Fig. 17b indicates wave surfaces above mountain barrier in a layer between the surface and the critical level (where wind direction changes from easterly to westerly), without signs of a hydraulic jump (Long 1954).

In addition to high winds, showers were reported throughout the state of Hawaii. On the island of Oahu, the Koolau Range received more than 30 mm of rainfall during the 24-h period ending at 0000 HST 15 February with 44 mm of rain recorded on its southeastern section (Fig. 18a). The Waianae Range, on the other hand, received little rainfall from this event even though trade winds were fairly strong at its ridge (see Fig. 17b). This is probably due to the effect of orographic moisture extraction by the Koolau Range to the east (Schroeder et al. 1977). For this case, the RSM/LSM forecasted no rain for the island of Oahu (not shown). Nevertheless, in the MSM/LSM simulations (Fig. 18b), appreciable rains were simulated along the windward side of the Koolau Range with no rain on the windward side of the Waianae Range, in general agreement with observations. The improvement of the MSM/LSM over the RSM/LSM during this event once again demonstrates the necessity of using high-resolution mesoscale model to better resolve island effects. Two deficiencies are noted in the MSM/LSM simulations: (1) the model forecast rainfall amount on the windward side of the Koolau Range was about twice as much as that observed; and (2) the model failed to generate the observed large amount of rainfall along the mountain ridge and its immediate leeside.

4. Summary

Over the island of Oahu, the coupled MSM/LSM performs better than the MSM in simulating 2-m temperature, 2-m dew point temperature, 10-m wind speed and 10-m wind direction during the period of May 20 through June 20 2002. The daytime cold bias and over-estimation of surface wind speed in the RSM and MSM simulations are corrected by coupling the MSM with the LSM. Sea breezes during weak trade wind days are also better simulated by the MSM/LSM than the MSM.
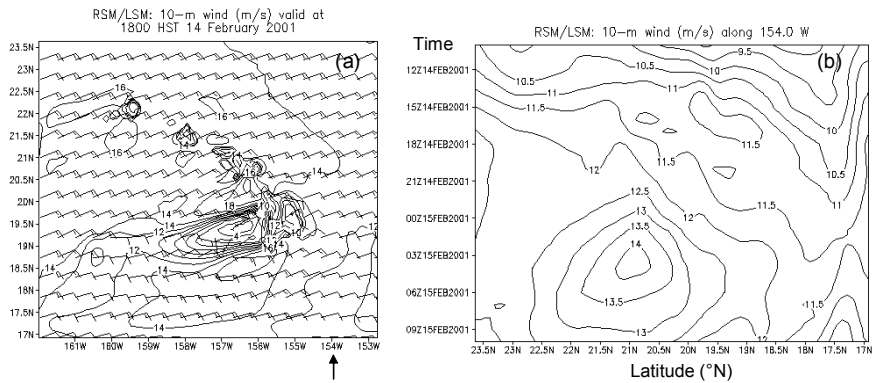
Fig. 16 (a) RSM/LSM 28-h forecast 10-m wind (m s^{-1}) valid at 1800 HST February 14 2001, and (b) Time-Latitude cross section along 154 °W featuring the RSM/LSM forecast 10-m wind (m s^{-1}). Time goes from 0000 HST February 14 (top) to 0000 HST February 15 (bottom). The position of the cross section is shown in (a) by an arrow. Isotaches are drawn for every 2 and 0.5 m s^{-1} in (a) and (b), respectively. Major features in (a) include (1) weak winds on the windward side due to island blocking; (2) wake areas of major islands; and (3) strong winds at the southern and northern corners of major islands as well as within the channels. Wind pattern over Kauai and Oahu appeared to be quite flat due to the coarse representation of the islands' terrain by the 10-km RSM grid. In (b), the strongest upstream winds occur around 1800 HST February 14. The RSM/LSM was initialized at 1400 HST February 13 2001.
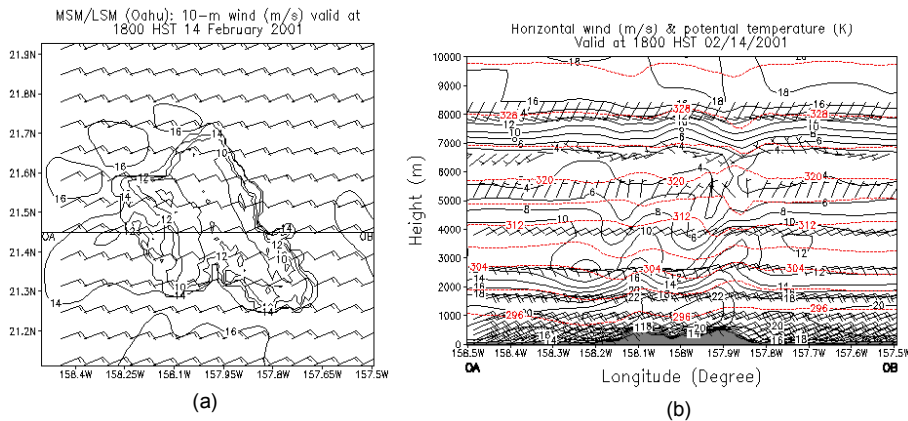

Fig. 17 (a) 10-m wind (m s^{-1}) over the Oahu domain and (b) longitude-height cross section along OA-OB showing horizontal wind (barbs and black lines) and potential temperature (red lines) constructed from the 1.5-km MSM/LSM 28-h forecast valid at 1800 HST February 14. Isotaches are drawn for every 2 m s^{-1}. The model terrain in this cross section is characterized by two north-south running mountains with peak height of 0.6 km. Notice the strong downslope winds (~ 22 m s^{-1}) along the lee slopes of both mountains, consistent with damage reports. The MSM/LSM was initialized at 1400 HST February 13 2001.

The high-resolution (≤ 3 km), coupled MSM/LSM shows significant improvement over the 10-km RSM in our case studies in simulating rainfall distribution, rainfall rate and airflows in association with heavy rainfall and high wind events. Nevertheless, the MSM/LSM over-predicts precipitation on the windward side of steep terrain while under-predicts precipitation on the lee side.

Future work will include: (1) extending the experimental daily forecasts to the Kauai domain and Hawaii-Maui-Molokai domain, (2) performing model sensitivity tests of cloud and precipitation schemes, and (3) conducting case studies and experimental high-resolution runs using the WRF model over the Hawaiian Islands.

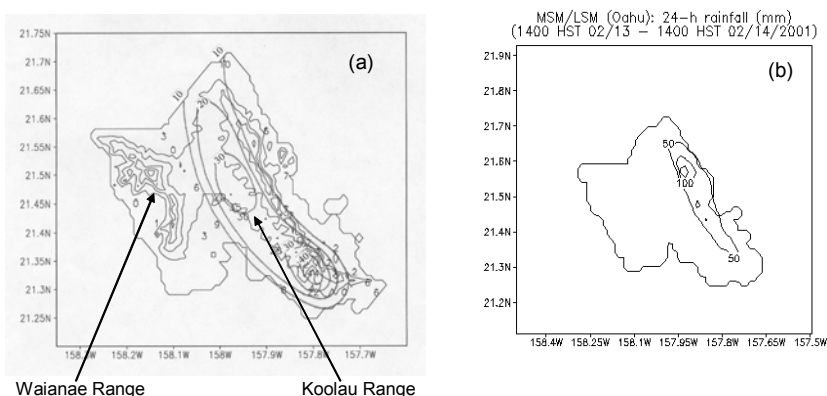Waianae Range   Koolau Range

Fig. 18 24-h accumulated rainfall (mm) from 1400 HST February 13 to 1400 HST February 14 2001 on the island of Oahu: (a) observed, and (b) simulated by the 1.5-km MSM/LSM. Contour interval is 10 mm in (a) and 50 mm in (b). The MSM/LSM was initialized at 1400 HST February 13. The MSM/LSM captured large amount of rainfall on the windward side, consistent with the observed local climate, but it failed to bring rains further upslope and leeward as indicated in observations. The heaviest rainfall amount in model simulations is about two times larger than in observations. The windward side of the Koolau Range is rather steep.

REFERENCES

Asselin, R. A., 1972: Frequency filter for time integration. *Mon. Wea. Rev.*, **100**, 487-490.

Avissar, R., and R. Pielke, 1989: A parameterization of heterogeneous land surfaces for atmospheric numerical models and its impact on regional meteorology. *Mon. Wea. Rev.*, **117**, 2113-2136.

Businger, S., T. Birchard Jr., P. A. Jendrowski, K. Kodama, J. N. Porter, and J.-J. Wang, 1998: A bow echo and severe weather associated with a Kona low in Hawaii. *Wea. Forecasting*, **13**, 579-591.

Chen, F., and R. Avissar, 1994a: The impact of land-surface wetness on mesoscale heat fluxes. *J. Appl. Meteor.*, **33**, 1324-1340.

—, and —, 1994b: Impact of land-surface moisture variability on local shallow convective cumulus and precipitation in large-scale models. *J. Appl. Meteor.*, **33**, 1382-1401.

—, and J. Dudhia, 2001a: Coupling an advanced land surface-hydrology model with the Penn State-NCAR MM5 modeling system. Part I: Model implementation and sensitivity. *Mon. Wea. Rev.*, **129**, 569-585.

—, and —, 2001b: Coupling an advanced land surface-hydrology model with the Penn State-NCAR MM5 modeling system. Part II: Preliminary model validation. *Mon. Wea. Rev.*, **129**, 587-604.

Chen, Y.-L., H.-M. H. Juang, P. A. Jendrowski, and K. Kodama, 1999: Application of the NCEP nonhydrostatic spectral model to improve weather forecasting in Hawaii. The 1st Regional Spectral Model Workshop, Maui, Hawaii, 9-13 August, 1999.

—, Y.-X. Zhang, H.-M. H. Juang, S.-Y. Hong, and K. Kodama, 2002: Application of the coupled surface model and mesoscale spectral model for the Hawaiian Islands. The 4th Regional Spectral Model Workshop, Los Alamos, New Mexico, July 31 – August 2, 2002.

DOI USGS 1986: Land Use Land Cover Digital Data from 1:250,000- and 1:100,000-Scale Maps. Data User Guide 4, U.S. Geological Survey, Reston, VA.

Hong, S.-Y., and H.-L. Pan, 1998a: Convective trigger function for a mass-flux cumulus parameterization scheme. *Mon. Wea. Rev.*, **126**, 2599-2620.

—, H.-M. H. Juang, and Q. Zhao, 1998b: Implementation of prognostic cloud scheme for a regional spectral model. *Mon. Wea. Rev.*, **126**, 2621-2639.

Juang, H.-M. H., 1992: A spectral fully compressible nonhydrostatic mesoscale model in hydrostatic sigma coordinates: Formulation and preliminary results. *Meteor. Atmos. Phys.*, **50**, 75-88.

—, and M. Kanamitsu, 1994: The NMC nested regional spectral model. *Mon. Wea. Rev.*, **122**, 3-26.

—, 2000: The NCEP mesoscale spectral model: A revised version of the nonhydrostatic regional spectral model. *Mon. Wea. Rev.*, **128**, 2329-2362.

—, C.-T. Lee, Y.-X. Zhang, Y. Song, M.-C. Wu, Y.-L. Chen, K. Kodama, and S.-C. Chen, 2003: Applying

horizontal diffusion on pressure surface to mesoscale models on terrain-following coordinates. Submitted.

Juvik, J. O., D. C. Singleton, and G. G. Clarke, 1978: Climate and water vapor on the island of Hawaii. Mauna Loa Observatory, Ed. J. Miller, Twentieth Anniversary Report, U. S. Department of Commence, NOAA, Environmental Research Lab., 129-139.

Kanamitsu, M., 1989: Description of the NMC global data assimilation and forecast system. *Wea. Forecasting*, **4**, 335-342.

Long, R. R., 1954: Some aspects of the flow of stratified fluids. Part II: Experiments with a two fluid system. *Tellus*, **6**, 97-115.

Mahrt, L., and H.-L. Pan, 1984: A two layer model of soil hydrology. *Bound.-Layer Meteor.*, **29**, 1-20.

Pan, H.-L., and L. Mahrt, 1987: Interaction between soil hydrology and boundary layer developments. *Bound.-Layer Meteo.*, **38**, 195-202.

Ramage, C. S., 1962: The subtropical cyclone. *J. Geophys. Res.*, **67**, 1401-1411.

Schroeder, T. A., B. J. Kilonsky, and B. N. Meisner, 1977: Diurnal variation in rainfall and cloudiness. UH-MET 77-03, Dept. of Meteorology, University of Hawaii. [Available from the Department of Meteorology, University of Hawaii, 2525 Correa Road, HI 96922, Honolulu]

Simpson, R. H., 1952: Evolution of the Kona storm: A subtropical cyclone. *J. Meteor.*, **9**, 24-35.

Wang, J.-J., H.-M. H. Juang, K. Kodama, S. Businger, Y.-L. Chen, and J. Partain, 1998: Application of the NCEP Regional Spectral Model to improve mesoscale weather forecasts in Hawaii. *Wea. Forecasting*, **13**, 560-575.

Zhang, Y.-X., Y.-L. Chen, H.-M. H. Juang, S.-Y. Hong, K. Kodama, and R. Farrell, 2000: Validation and sensitivity tests of the Mesoscale Spectral Model simulations over the Hawaiian Islands. The 2nd Regional Spectral Model Workshop, Maui, Hawaii, 17-21 July, 2000.